applied sciences

MDPI

Article

Investigation of Frequency-Dependent Characteristics of Wire Rope under Tension Based on Transfer Function Method

Kwanghun Jeong †, Narae Kim †, Nahyun Jeon, Haksung Kim and Junhong Park *

School of Mechanical Engineering, Hanyang University, Seoul 04763, Republic of Korea; zjavbfk@hanyang.ac.kr (K.J.); dogmecome@hanyang.ac.kr (N.K.); nahyun.j11@gmail.com (N.J.); kima@hanyang.ac.kr (H.K.)

* Correspondence: parkj@hanyang.ac.kr; Tel.: +82-2-2220-0424

† These authors contributed equally to this work.

Abstract: Wire rope is a complex structure made by twisting wires of various sizes in the longitudinal direction. It is used to support or move engineering structures and is subject to various tensions. Dynamic properties are important parameters to evaluate the resistance to bending deformation and vibration reduction of various structures. They are affected by the magnitude of tension. In this study, an experimental method for measuring the frequency-dependent characteristics of wire rope under tension is proposed. The study analyzed flexural wave propagation employing a vibration transfer function. Experimental results showed that the transfer function of wire rope under tension is affected by tension and bending stiffness. The Newton–Raphson method was employed to numerically measure wavenumbers of the wire rope. The bending stiffness and loss factor were determined from the wavenumbers. Changes in the bending stiffness and loss factor as the tension increased were explained by the dynamic behavior of the structure under tension. As the tension increased, the bending stiffness increased, and the loss factor decreased. Hysteresis analysis indicated that the energy dissipation of wire rope is greater than that of a steel beam due to the friction between the wires. Statistical analysis confirmed a significant correlation between dynamic characteristics and tension in wire rope.

Keywords: wire rope; dynamic characteristics; tension; transfer function method

Citation: Jeong, K.; Kim, N.; Jeon, N.; Kim, H.; Park, J. Investigation of Frequency-Dependent Characteristics of Wire Rope under Tension Based on Transfer Function Method. *Appl. Sci.* **2024**, *14*, 4621. https://doi.org/10.3390/app14114621

Academic Editor: Rosario Pecora

Received: 8 May 2024
Revised: 22 May 2024
Accepted: 24 May 2024
Published: 28 May 2024

1. Introduction

A wire rope is a structure made by twisting several strands around a core. Each strand is composed of twisted steel wires. Wire ropes with high strength and flexibility are widely used in various industrial sites such as construction, shipbuilding, and manufacturing plants [1]. In particular, wire ropes are mainly used to move and support structures such as large suspension bridges, elevators, cranes, and cable cars [2]. Exposed to external shocks in their operational environment, wire ropes are susceptible to bending and vibration. Mitigating bending and vibration is crucial for maintaining the structural integrity of wire ropes and their connected structures. Bending stiffness and loss factor are important dynamic properties for evaluating resistance to bending and vibration damping. Because wire rope is subjected to various tensions, it is necessary to investigate its dynamic properties for various tensions.

It is important to investigate the change in bending stiffness when a wire rope is bent or stretched. This change results from friction and relative movement among the wires. The bending stiffness changed with the slip between the wires [3]. When there was no slippage between the wires, they were glued and moved together. The wire rope behaved like a rigid beam, and it had the maximum bending stiffness. Additionally, the friction property of the wire rope was reduced due to no slippage between the wires [4]. The static friction between the wires was overcome, and the bending stiffness began to decrease as

the wires slid. It had the lowest bending stiffness when all wires slid completely. When the wire rope transitioned from a loose state to a solid state, its moment of inertia increased [5]. The maximum bending stiffness appeared at high tension and low curvature [6]. The high tension made the wire rope more like a rigid beam, and the wires were glued together rather than sliding. As the tension was applied to the wire rope, a normal force was generated between the wires [7]. The sliding friction along the contact line between the wires was proportional to the normal force. Friction serves as an effective vibration damping mechanism, transforming kinetic energy into thermal energy. The friction due to relative motion between wires causes large damping. Scanning electron microscope micrographs were used to analyze individual wire wear in steel wire rope [8]. Frictional wear of the core wire was large, and the friction dissipated a large amount of energy. Most of the energy dissipation in the wire rope was caused by friction between the wires [9]. The damping was much greater in a wire rope, where friction could occur, than in a single wire. The steel wire rope degradation mechanisms and damage detection methods highlight the importance of understanding frictional interactions and wear in wire ropes [10].

Several studies have been developed to measure the vibration damping of wire ropes and their associated structures. The damping of a cable-stayed bridge model was measured using damped harmonic vibration caused by excitation with a hand-held shaker. The damping value for the main mode was calculated from the attenuation curves based on exponential curve fitting in the time domain [11]. The damping ratio of the stay cable was calculated through vibration modal analysis, and the vibration was measured using a video camera and a laser Doppler vibrometer [12]. The bending stiffness and vibration damping of the wire rope were investigated according to the applied static tension [13]. The damping ratio of each mode was calculated through modal parameter analysis in the frequency domain, and the damping ratio decreased as the tension increased. The bending stiffness and material damping were estimated based on the maximum a posteriori estimator with a frequency response function [14]. The effective bending stiffness of the cable was calculated based on the simply supported beam theory [15]. The lateral impact performance of wire ropes was studied to understand the wire ropes' dynamic behavior under various conditions, including tension and side impacts [16].

In many studies, the wire rope was modeled as an Euler beam under tension. The vibration response of a tensioned Euler beam was theoretically solved under various boundary conditions [17]. The Euler beam-based distributed transfer function method has been developed to model the vibrational response of wire rope and cable structures [18]. The model included shear effect, tension, and hysteresis damping of helical strands. The tensioned cable was modeled as a Euler beam, and the axial force, bending stiffness, and rotational stiffness were investigated using its natural frequencies and modes [19]. The first few natural frequencies were used to investigate the axial force and bending stiffness in the cable model [20]. The transfer function method has been used to investigate dynamic characteristics for various structures. The dynamic properties of the complex structure beams were measured based on the transfer function method. To analyze the vibrations of sandwich beams of different core materials and a polymer beam, flexural wave propagations were analyzed using the Timoshenko beam theory and Euler beam theory [21]. In a recent study, a detailed mechanical analysis of a wire rope under tension was performed, and the experimental results were verified using a finite element model [22].

Structures are subjected to various tensions over time, and their bending deformation and vibration damping are important factors for safety and lifespan. In this study, the dynamic characteristics of the wire rope under tension were measured using the transfer function method. The flexural wave propagation was analyzed based on the Euler beam theory. A wire rope and steel beam were used in experiment. A universal testing machine applied a static load to the specimen, and a vibrating shaker excited random vibrations. The vibration response was measured using two accelerometers. The steel beam was used to measure the translational and rotational stiffness of the boundary conditions and compare the dynamic characteristics of the wire rope. The frequency-dependent bending stiffness

and loss factor were measured with increasing tension. For the wire rope, the bending stiffness increased and the loss factor decreased as the tension increased. A regression model was employed to determine the correlation between tension and dynamic characteristics. Statistical validation was conducted to confirm the performance and significance of the regression model. The regression model can be used for predicting dynamic behavior for arbitrary tensions.

2. Wire Rope Flexural Vibration Modeling

The flexural vibration of a wire rope under tension is analyzed based on the Euler beam model. The dynamic characteristics of the wire rope under tension are measured through flexural vibration. Figure 1 shows a spring-supported Euler beam model under tension. The ends are supported by the translational spring k_T and the rotational spring k_R. The static tension T is applied to the beam of length L. Force F is applied at a distance L_f from the left clamp end to excite the beam. The equation of motion for the Euler beam under tension is given as follows:

$$D\frac{\partial^4 w}{\partial x^4} - T\frac{\partial^2 w}{\partial x^2} + M_b\frac{\partial^2 w}{\partial t^2} = 0, \tag{1}$$

where w is transverse displacement, D is bending stiffness, and M_b is mass per unit length.

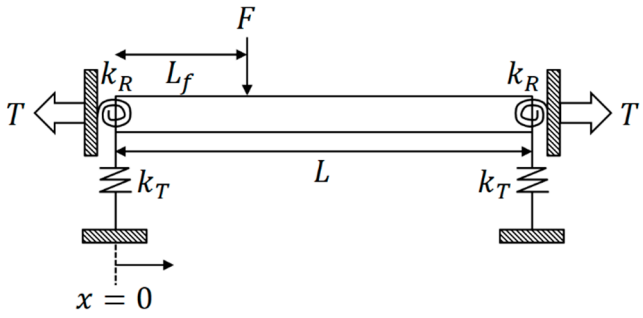

Figure 1. Spring-supported Euler beam model under tension.

When a force is applied to the middle of the beam, the beam function satisfying Equation (1) is given as follows:

$$\begin{gathered}\hat{w}(x) = \begin{cases}\hat{w}_1(x) & 0 \le x \le L_f \\ \hat{w}_2(x) & L_f \le x \le L\end{cases}, \\ \hat{w}_1(x) = \hat{A}_1 \sin \hat{M}x + \hat{A}_2 \cos \hat{M}x + \hat{A}_3 e^{\hat{N}x} + \hat{A}_4 e^{-\hat{N}x}, \\ \hat{w}_2(x) = \hat{A}_5 \sin \hat{M}\left(x - L_f\right) + \hat{A}_6 \cos \hat{M}\left(x - L_f\right) + \hat{A}_7 e^{\hat{N}(x-L_f)} + \hat{A}_8 e^{-\hat{N}(x-L_f)},\end{gathered} \tag{2}$$

$$\begin{pmatrix}\hat{M} \\ \hat{N}\end{pmatrix} = \left[\mp\hat{t} + \left(\hat{t}^2 + \hat{b}^2\right)^{1/2}\right]^{1/2}, \tag{3}$$

$$\hat{t} = T/2\hat{D} = T\hat{b}^2/2M_b\omega, \quad \hat{b} = \left(M_b\omega^2/\hat{D}\right)^{1/2}, \quad \hat{D} = D(1 + i\eta), \tag{4}$$

where $\hat{A}_1$–$\hat{A}_8$ are complex amplitude coefficients, $\hat{M}$ and $\hat{N}$ are wavenumbers ($\hat{M} = M_r - iM_i$, $\hat{N} = N_r - iN_i$), ω is angular frequency, $\hat{D}$ is complex bending stiffness, η is loss factor, and H is the Heaviside step function.

To obtain a general solution for the wave equation satisfying Equation (2), it is necessary to solve for the unknown coefficients. Eight boundary conditions are used to determine the coefficients as follows:

$$\begin{gathered}
\hat{D}\frac{\partial^2\hat{w}_1(0)}{\partial x^2} = k_R\frac{\partial\hat{w}_1(0)}{\partial x}, \\
\hat{D}\frac{\partial^3\hat{w}_1(0)}{\partial x^3} = -k_T\hat{w}_1(0), \\
\hat{w}_1(L_f) = \hat{w}_2(L_f), \\
\frac{\partial\hat{w}_1(L_f)}{\partial x} = \frac{\partial\hat{w}_2(L_f)}{\partial x}, \\
\hat{D}\frac{\partial^2\hat{w}_1(L_f)}{\partial x^2} = \hat{D}\frac{\partial^2\hat{w}_2(L_f)}{\partial x^2}, \\
\hat{D}\frac{\partial^3\hat{w}_1(L_f)}{\partial x^3} + T\frac{\partial\hat{w}_1(L_f))}{\partial x} + T\frac{\partial\hat{w}_2(L_f))}{\partial x} - \hat{D}\frac{\partial^3\hat{w}_2(L_f)}{\partial x^3} = F, \\
\hat{D}\frac{\partial^2\hat{w}_2(L)}{\partial x^2} = -k_R\frac{\partial\hat{w}_2(L)}{\partial x}, \\
\hat{D}\frac{\partial^3\hat{w}_2(L)}{\partial x^3} = k_T\hat{w}_2(L),
\end{gathered} \tag{5}$$

The eight equations are rearranged, and the unknown complex amplitude coefficients are solved via symbolic calculation. The transfer function for the tensioned beam displacement is used to measure the wavenumbers, and it is expressed as follows:

$$\Lambda e^{i\phi} = \frac{\hat{w}(x_2)}{\hat{w}(x_1)}, \tag{6}$$

where Λ and ϕ are the amplitude and phase of the measured transfer function, and x_1 and x_2 are the vibration measurement locations.

The unknown frequency parameter $\hat{b} = b_r - ib_i$ is calculated using the transfer function method as follows:

$$\begin{bmatrix} b_r \\ b_i \end{bmatrix}_{j+1} = \begin{bmatrix} b_r \\ b_i \end{bmatrix}_j - \begin{bmatrix} \mathrm{Re}\left\{\frac{\partial\hat{w}(x_2)}{\partial b_r}, \frac{\partial\hat{w}(x_2)}{\partial b_i}\right\} \\ \mathrm{Im}\left\{\frac{\partial\hat{w}(x_2)}{\partial b_r}, \frac{\partial\hat{w}(x_2)}{\partial b_i}\right\} \end{bmatrix}^{-1} \begin{bmatrix} \mathrm{Re}\left\{\hat{w}(x_2) - \hat{w}(x_1)\Lambda e^{i\phi}\right\} \\ \mathrm{Im}\left\{\hat{w}(x_2) - \hat{w}(x_1)\Lambda e^{i\phi}\right\} \end{bmatrix}, \tag{7}$$

By calculating the unknown frequency parameter $\hat{b}$, the wavenumbers $\hat{M}$ and $\hat{N}$ are determined. In addition, the bending stiffness and loss factor with frequency are determined as follows:

$$\hat{D} = M_b\omega^2/\hat{b}^2, \tag{8}$$

3. Experimental Setup for Wire Rope Vibration Measurement under Tension

The widely used 19 × 7 construction wire rope was selected to investigate the vibration dynamic characteristics under tension. The wire rope was composed of steel, and it had a diameter of 8 mm, a length of 200 mm, a cross section of 29.70 mm^2, a mass per length of 0.27 kg/m, and an elastic modulus of 200 GPa. Figure 2 shows the structure of the wire rope used in the experiment. The wire rope had 19 strands, and each strand consisted of 7 wires. To investigate the effect of tension on the vibration of the wire rope, a static load was applied to the wire rope using a universal testing machine (RB301 UNITECH-M, R&B Co., Ltd., Daejeon, Republic of Korea). In order to compare with the wire rope structure, the dynamic characteristics of the steel beam were additionally investigated. The steel beam had a width of 30 mm, a thickness of 3 mm, a length of 200 mm, and an elastic modulus of 200 GPa. Figure 3 shows the experimental setup for the vibration measurement of the steel beam and wire rope under tensile test. They were supported by both jigs and excited by a small vibration shaker. The vibration was measured by the two accelerometers. For the steel beam, the vibration shaker and the accelerometers were attached at 2.4, 5.0, and 6.8 cm from the end, respectively. Tensions of 1, 2, 3, 4, and 5 kN were applied to the steel beam and wire rope. A Fourier transform analyzer (3560-B-030, B&K Inc., Brodhagen, ON, Canada) was used to measure the vibration transfer function with the tensions.

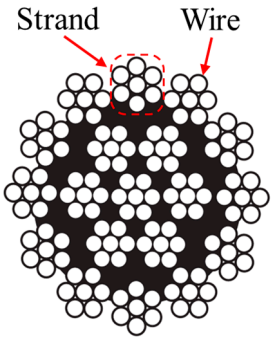

Figure 2. Structure of the wire rope used in the experiment. The wire rope had 19 strands, and one strand consisted of seven wires.

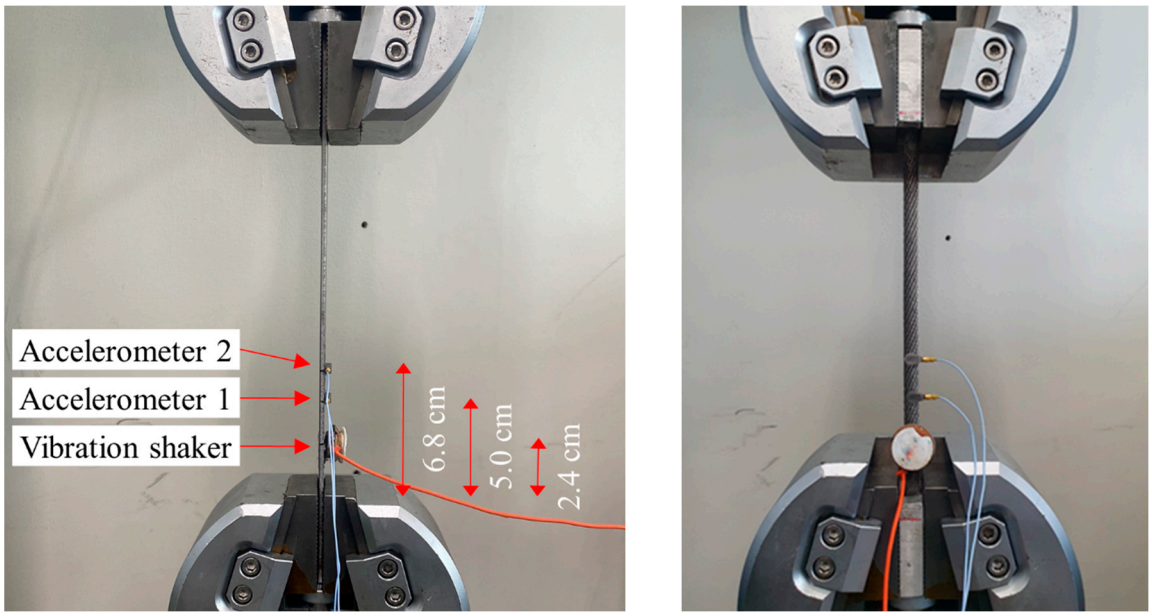

(**a**) (**b**)

Figure 3. Experimental setup for the vibration measurement of (**a**) the steel beam and (**b**) the wire rope under a tensile test. They were supported by both jigs and excited by a small vibration shaker. The vibration shaker and the accelerometers were attached at 2.4, 5.0, and 6.8 cm from the end, respectively.

4. Experimental Results and Analysis

4.1. Wire Rope Wavenumber Analysis under Tension

Flexural vibration measurements were conducted to investigate the dynamic characteristics of the steel beam and wire rope under tension. A transfer function was obtained from the flexural vibrations measured by the accelerometers. Figure 4 shows the measured and predicted transfer functions of the steel beam without tension in the frequency range of 400–2000 Hz. The transfer functions were used to calculate the translational and rotational spring stiffness of the joint between the specimen and the jig. They were 4.5 MN/m and 4.2 kNm/rad. Figure 5 shows the measured and predicted transfer functions of the wire rope under tensions in the frequency range of 200–2000 Hz. The measured and predicted transfer functions exhibited similarity for the wire rope without tension. As the tension increased from 0 to 1 kN, the predicted transfer function from the Euler beam model shifted to the right due to the effect of the applied tension. However, the measured transfer function with a tension of 1 kN shifted further to the right than the predicted transfer function. This indicated that the dynamic properties of wire rope were more sensitive to tensions compared to the steel beam. The difference between the predicted and measured transfer

functions was attributed to the change in bending stiffness. The vibration transfer function of the specimens under tension was affected by tension and bending stiffness factors.

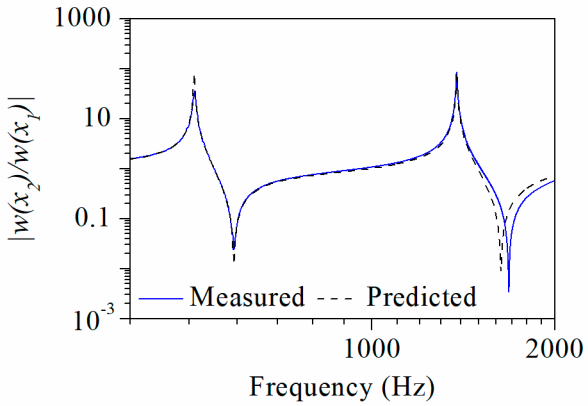

Figure 4. Measured and predicted transfer functions without tension of the steel beam in the frequency range of 400–2000 Hz. The transfer functions were used to calculate the translational and rotational spring stiffness of the joint between the specimen and the jig.

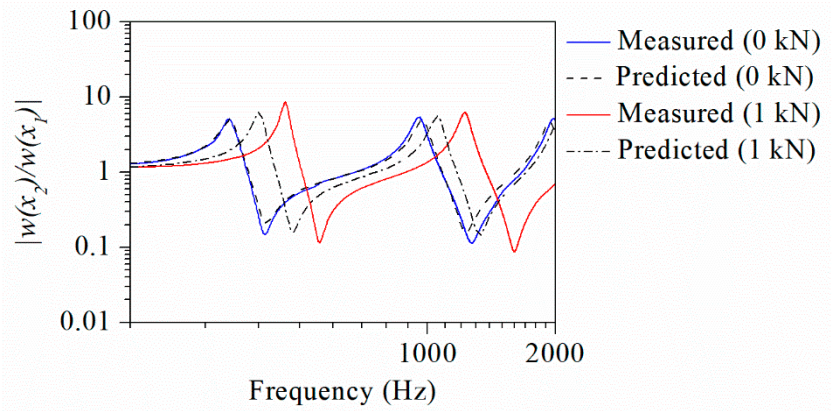

Figure 5. Measured and predicted transfer functions of the wire rope with tensions in the frequency range of 200–2000 Hz.

Figure 6 shows the vibration transfer function of the steel beam and wire rope with tensions. The transfer functions of the steel beam and wire rope were measured in the frequency ranges of 400–2000 and 200–2000 Hz. As the tension increased, the transfer function of the steel beam and wire rope shifted to the right. It was influenced by changes in the tension and bending stiffness. The wavenumbers with frequency were measured from the transfer function method. Figure 7 shows the measured wavenumbers of the steel beam and wire rope under various tensions. There were two wavenumbers, M and N, in the specimens due to tension. The harmonic wave's wavenumber, $\hat{M}$, held greater significance compared to the non-harmonic wave's wavenumber, $\hat{N}$. The investigation was focused on the harmonic wave's wavenumber, M. As the frequency increased, the values of the wavenumbers showed a tendency to increase. As the tension increased, the values of the wavenumbers M_r and M_i showed a clear tendency to decrease. Flexural wave speed c_M was calculated by dividing angular frequency ω by the wavenumber M_r, as represented by $c_M = \omega / M_r$. Figure 8 shows the measured flexural wave speed of the steel beam and wire rope with tensions. The flexural wave speed was dependent on the frequency. As the frequency increased, the values of the flexural wave speed showed a tendency to increase. As tension increased, the flexural wave speed increased in both solid beam and wire rope structures.

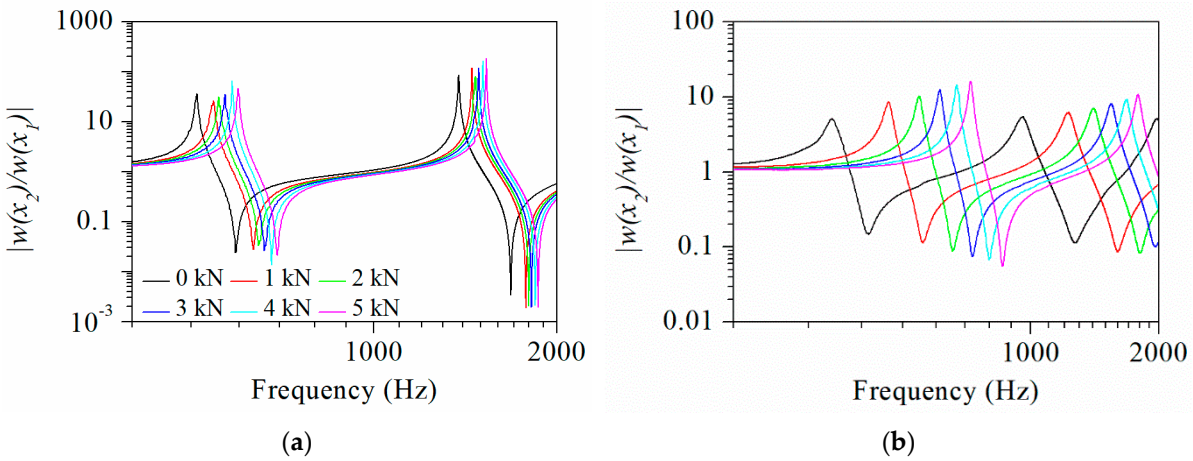

Figure 6. Vibration transfer functions of (**a**) steel beam and (**b**) wire rope with tensions. As the tension increased, the transfer function shifted to the right. It was influenced by changes in the tension and bending stiffness.

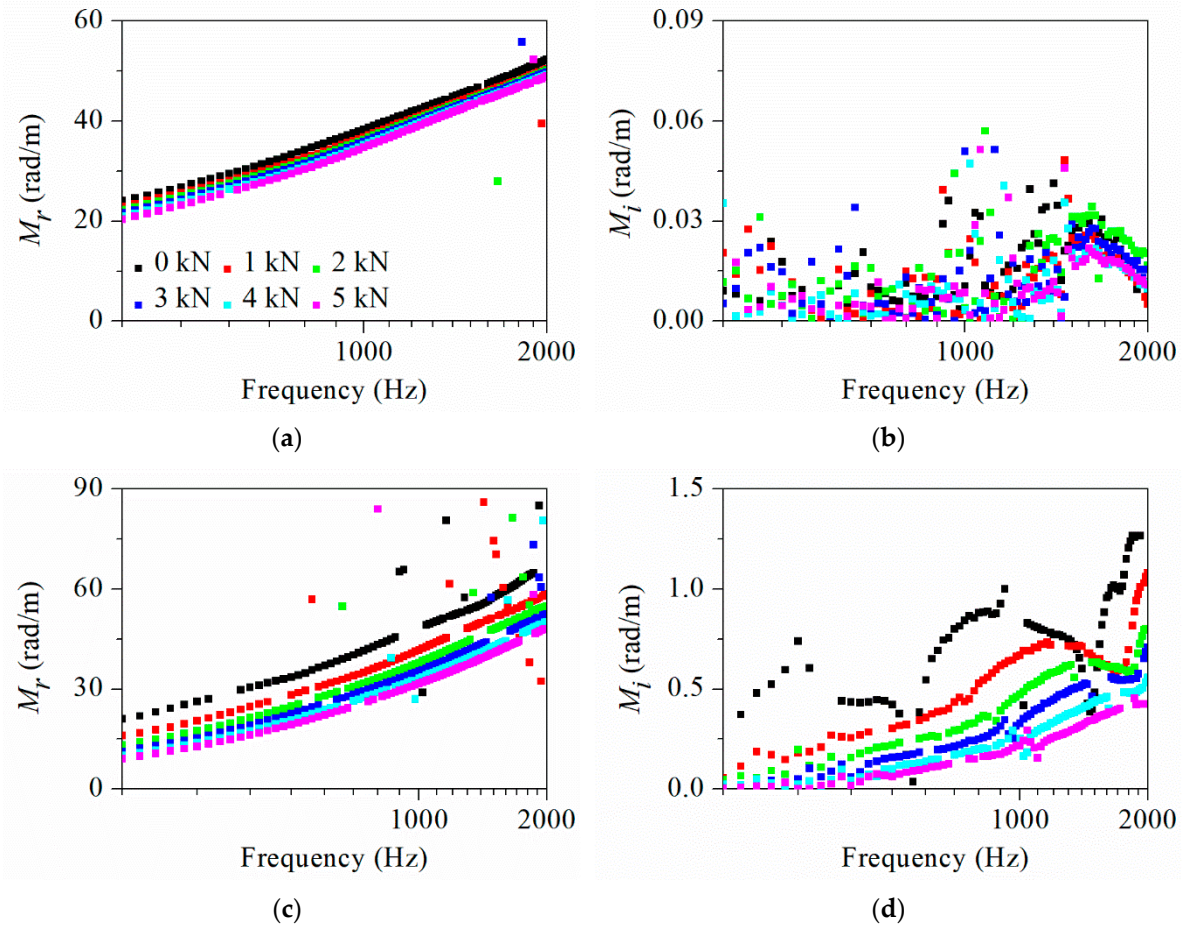

Figure 7. Measured complex wavenumbers of a (**a**,**b**) steel beam and (**c**,**d**) wire rope with tensions. As the frequency increases, the values of the wavenumbers show a tendency to increase. As the tension increases, the values of the wavenumbers M_r and M_i show a clear tendency to decrease.

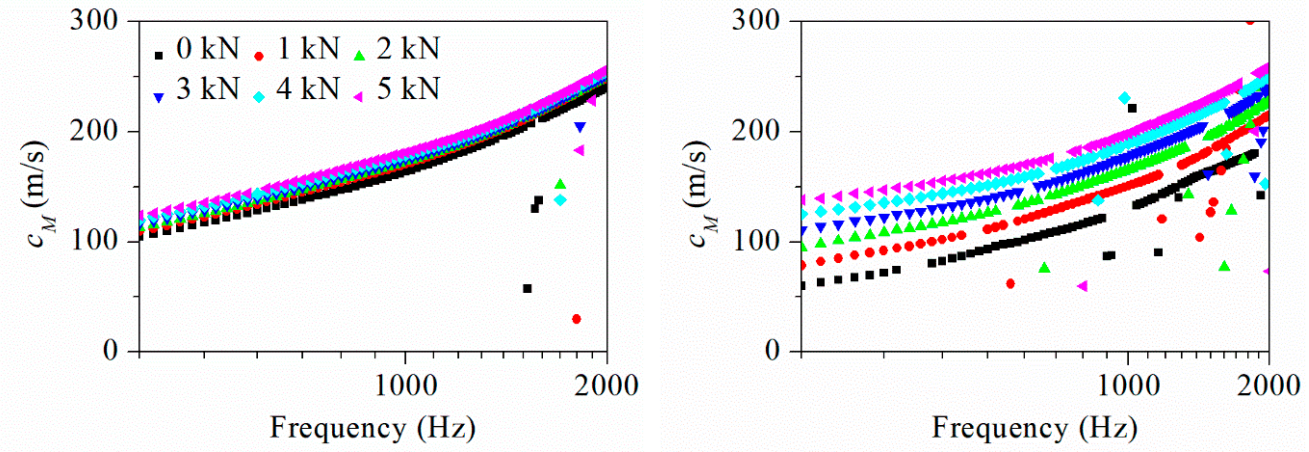

Figure 8. Measured flexural wave speed of a (**a**) steel beam and (**b**) wire rope with tensions. As the frequency increases, the values of the flexural wave speed show a tendency to increase. As tension increases, the flexural wave speed increases in both solid beam and wire rope structures.

4.2. Wire Rope Dynamic Characteristics Analysis under Tension

The dynamic characteristics of the steel beam and wire rope were analyzed with tensions. The wavenumbers were used to measure the dynamic characteristics, including bending stiffness and loss factor. Figure 9 shows the measured dynamic characteristics of the steel beam and wire rope with tensions. The bending stiffness and loss factor of the wire rope showed relatively large changes as the tension increased compared to the steel beam. The moment of inertia was important because the bending stiffness was determined by an elastic modulus and the moment of inertia. The steel beam, being in a solid state, exhibited minimal changes in the moment of inertia as the tension increased. The bending stiffness of the wire rope showed a relatively greater change as the tension increased than that of the steel beam. On the other hand, as the applied tension on the wire rope increased, it transitioned from a loose state to a solid state, resulting in a significant increase in the moment of inertia. The loss factor of the steel beam remained relatively unaffected by the increase in tension, whereas the loss factor of the wire rope showed a noticeable decreasing trend. As the tension increased, the wire rope transitioned from a loose state to a solid state, and the adhesion between wires and strands increased. The relative displacement between the wires and strands was reduced due to the strong adhesion, which reduced slippage between them. As sliding did not occur, the friction of the wire rope was reduced. Because friction was associated with energy dissipation, a decrease in friction led to reduced vibration damping. Unlike the wire rope structure, the steel beam structure had a weaker relationship between tension and friction. Therefore, the tendency of vibration damping with increasing tension did not appear clearly. Figure 10 shows the hysteresis curves of the steel beam and wire rope. The area of the hysteresis curve expresses the energy dissipated by internal friction. A large area of the hysteresis curve indicates a large vibration damping and loss factor. The measured hysteresis curve areas of the steel beam and wire rope were 0.11 and 0.24 MPa, and the area of the wire rope was larger than that of the steel beam. This indicated that the wire rope had a higher vibration damping and loss factor than the steel beam. This supported that the wire rope, being in a relatively loose state compared to the steel beam, exhibited greater energy dissipation due to friction. Figure 11 shows the average dynamic characteristic values of the steel beam and wire rope with tensions. A regression model was created to estimate the bending stiffness and loss factor with tensions. In the model, R^2 was used to measure the correlation between the independent and dependent variables, and the *p*-value was determined to evaluate the statistical significance. To ensure statistical significance of the model, the *p*-value must be lower than 0.05 [23]. In the steel beam, the R^2 and *p*-value were 0.643 and 0.055 for the bending stiffness, and they were

0.012 and 0.837 for the loss factor. Therefore, the bending stiffness and loss factor of the steel beam structure did not have a clear correlation with tensile force. As shown in Figure 4, regardless of the change in dynamic characteristics, the transfer function shifted to the right due to the increase in tensile force. In the wire rope, the R^2 and p-value were 0.995 and 9.75×10^{-6} for the bending stiffness, and they were 0.990 and 3.66×10^{-5} for the loss factor. Therefore, the dynamic characteristics of the wire rope structure had a clear correlation with tensile force. The bending stiffness of the wire rope increased from 2.20 to 5.49 Nm^2. The loss factor of the wire rope decreased from 0.062 to 0.038. Furthermore, the regression model developed for the wire rope facilitates predictions of bending stiffness and loss factor dependent on tension.

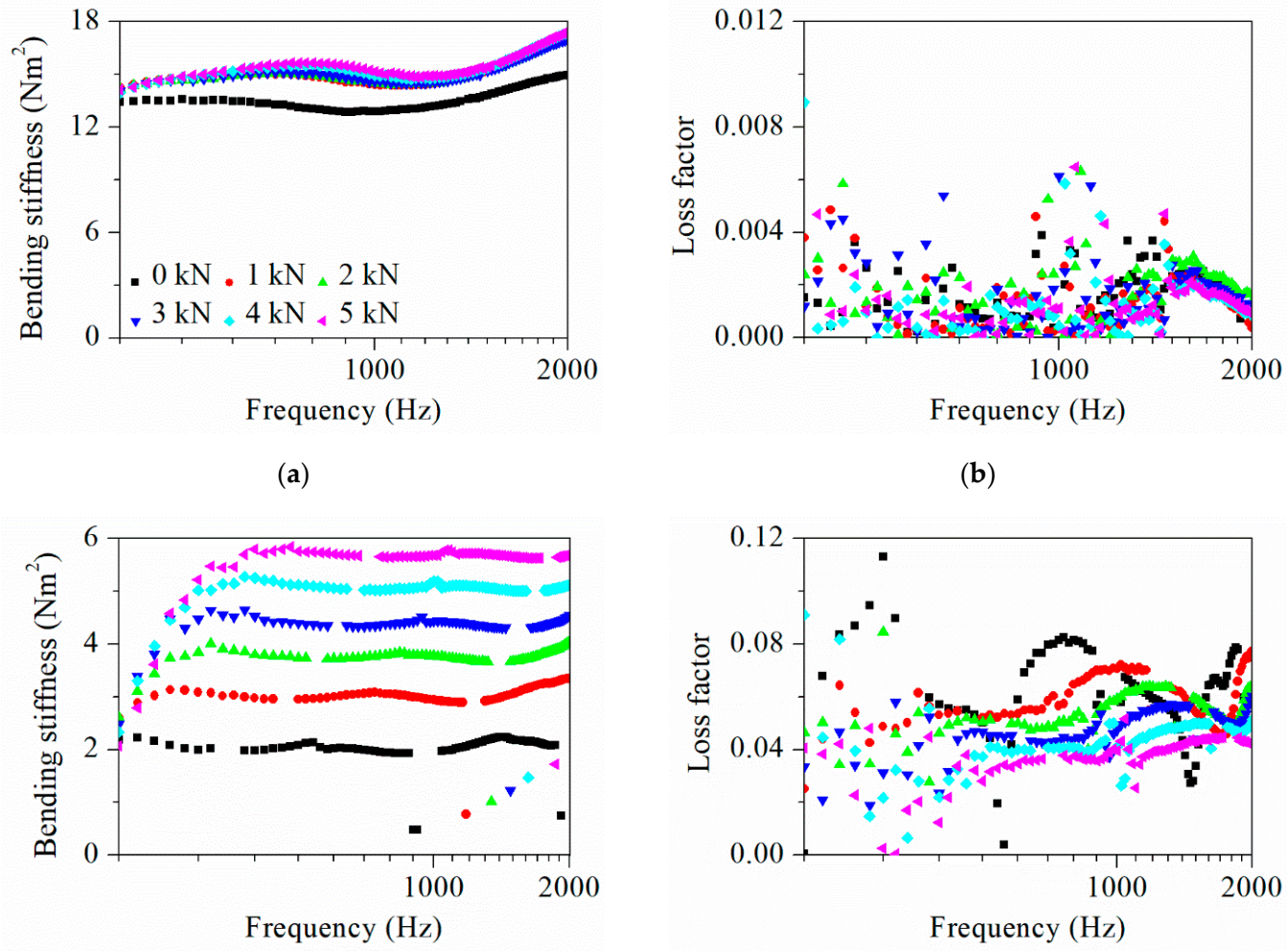

Figure 9. Measured dynamic characteristics of the steel beam and wire rope with tensions (kN); (**a**) bending stiffness and (**b**) loss factor of the steel beam. (**c**) Bending stiffness and (**d**) loss factor of the wire rope.

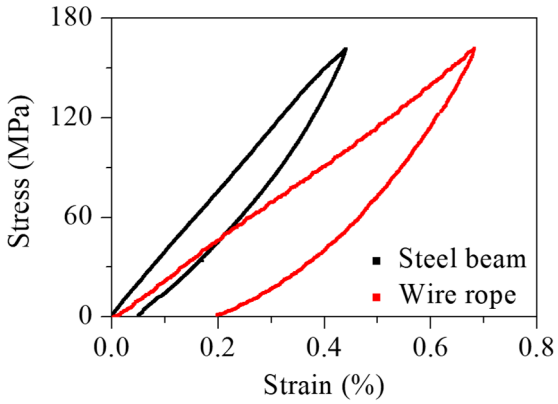

Figure 10. Hysteresis curves of the steel beam and wire rope. The area of the hysteresis curve expresses the energy dissipated by internal friction.

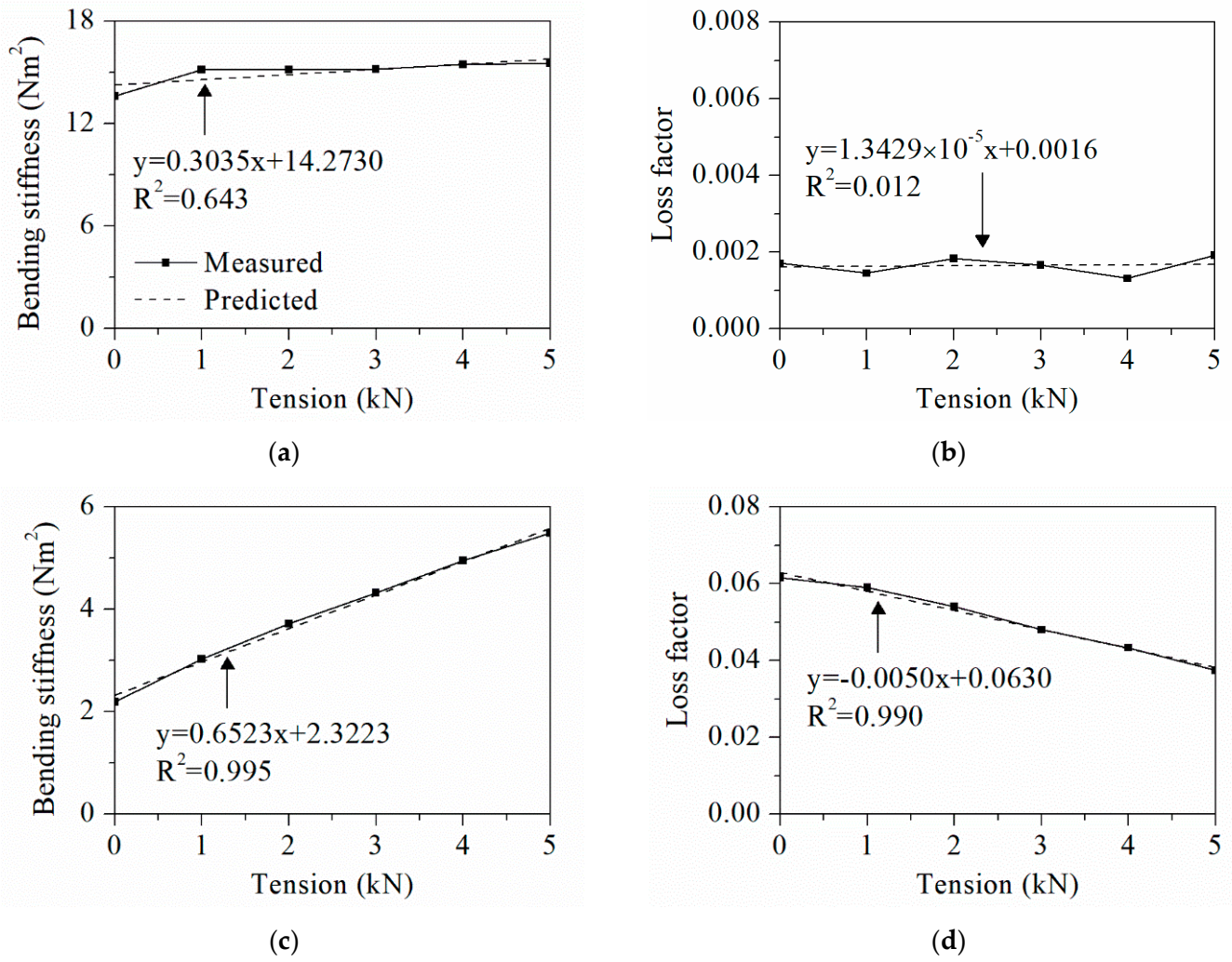

Figure 11. Average dynamic characteristic values of the steel beam and wire rope with tensions; (**a**) average bending stiffness and (**b**) loss factor of the steel beam. (**c**) Average bending stiffness and (**d**) loss factor of the wire rope. In the steel beam, the R^2 and p-value were 0.643 and 0.055 for the bending stiffness, and they were 0.012 and 0.837 for the loss factor. In the wire rope, the R^2 and p-value were 0.995 and 9.75×10^{-6} for the bending stiffness, and they were 0.990 and 3.66×10^{-5} for the loss factor.

5. Conclusions

In this study, an experimental methodology for measuring frequency-dependent characteristics of a wire rope structure under static tension was proposed. The transfer function method was employed to numerically measure the wavenumbers of the steel beam and wire rope. As the tension increased, the harmonic wave's wavenumber showed a clear tendency to decrease in the frequency domain. The bending stiffness and loss factor were obtained from the wavenumbers. The bending stiffness and the loss factor of the beam structure were not statistically correlated with tension. In the wire rope, the bending stiffness increased and the loss factor decreased as the tension increased. The hysteresis analysis showed that the wire rope exhibited higher energy dissipation compared to the steel beam due to friction between wires. Additionally, the performance and significance of the regression model for the wire rope were statistically verified. The proposed method can be applied to measure the dynamic characteristics of diverse structures under various tensions and to predict dynamic behavior for arbitrary tensions.

Author Contributions: K.J. and N.K. contributed equally to this article as first author. Conceptualization, K.J., N.K., N.J., H.K. and J.P.; Data curation, K.J., N.K. and N.J.; Formal analysis, K.J., N.K. and N.J.; Methodology, K.J., N.K. and N.J.; Writing—original draft, K.J. and N.K.; Writing—review & editing, K.J., N.K., N.J., H.K. and J.P. All authors have read and agreed to the published version of the manuscript.

Funding: This research was funded by the Korea Institute of Planning and Evaluation for Technology in Food, Agriculture, and Forestry (IPET) grant number [No. 322047051HD0e0, Development of 110 kW class large tractor based on eco-friendly hydrogen fuel cell].

Institutional Review Board Statement: Not applicable.

Informed Consent Statement: Not applicable.

Data Availability Statement: The original contributions presented in the study are included in the article, further inquiries can be directed to the corresponding author.

Conflicts of Interest: The authors declare no conflicts of interest.

References

1. Ouyang, Y.; Sun, H.; Jiang, S.; Hong, T.; Huang, Z.; Shu, S.; Chen, D.; Wang, T. Study on Damage Tests Based on Structure and Operating Parameters of Wire Ropes Used by Conveyors in Orchards. *J. Test. Eval.* **2021**, *49*, 2353–2369. [CrossRef]
2. Rostami, J.; Tse, P.W.; Yuan, M. Detection of broken wires in elevator wire ropes with ultrasonic guided waves and tone-burst wavelet. *Struct. Health Monit.* **2020**, *19*, 481–494. [CrossRef]
3. Papailiou, K.O. Bending of Helically Twisted Cables under Variable Bending Stiffness due to Internal Friction, Tensile Force and Cable Curvature. Ph.D. Thesis, ETH Zürich, Zürich, Switzerland, 1995.
4. Vinogradov, O.G.; Atatekin, I.S. Internal friction due to wire twist in bent cable. *J. Eng. Mech.* **1986**, *112*, 859–873. [CrossRef]
5. Oberg, E.; Jones, F.D.; Horton, H.L.; Ryffel, H.H.; Mccauley, C.J.; Heald, R.; Hussain, M.I. *Machinery's Handbook*; Industrial Press New York: New York, NY, USA, 1914; Volume 6.
6. Filiatrault, A.; Stearns, C. Flexural Properties of Flexible Conductors Interconnecting Electrical Substation Equipment. *J. Struct. Eng.* **2005**, *131*, 151–159. [CrossRef]
7. Ramsey, H. Analysis of interwire friction in multilayered cables under uniform extension and twisting. *Int. J. Mech. Sci.* **1990**, *32*, 709–716. [CrossRef]
8. Urchegui, M.A.; Tato, W.; Gómez, X. Wear Evolution in a Stranded Rope Subjected to Cyclic Bending. *J. Mater. Eng. Perform.* **2008**, *17*, 550–560. [CrossRef]
9. Yu, A.-t. Vibration Damping of Stranded Cable. Ph.D. Thesis, Lehigh University, Bethlehem, PA, USA, 1949.
10. Mazurek, P. A Comprehensive Review of Steel Wire Rope Degradation Mechanisms and Recent Damage Detection Methods. *Sustainability* **2023**, *15*, 5411. [CrossRef]
11. Garevski, M.A.; Severn, R.T. Damping and response measurement on A small-scale model of A cable-stayed bridge. *Earthq. Eng. Struct. Dyn.* **1993**, *22*, 13–29. [CrossRef]
12. Wangchuk, S.; Siringoringo, D.M.; Fujino, Y. Modal analysis and tension estimation of stay cables using noncontact vision-based motion magnification method. *Struct. Control Health Monit.* **2022**, *29*, e2597. [CrossRef]
13. Barbieri, N.; Júnior, O.H.d.S.; Barbieri, R. Dynamical analysis of transmission line cables. Part 1—Linear theory. *Mech. Syst. Signal Process.* **2004**, *18*, 659–669. [CrossRef]

14. Castello, D.A.; Matt, C.F.T. A validation metrics based model calibration applied on stranded cables. *J. Braz. Soc. Mech. Sci. Eng.* **2011**, *33*, 417–427. [CrossRef]
15. Guo, L.; Liu, H.; Chen, Z. Experimental research on the bending performance of locked coil wire rope and Galfan strand. *Constr. Build. Mater.* **2021**, *304*, 124667. [CrossRef]
16. Feng, Z.; Wang, X. Lateral impact performance of wire ropes. *Constr. Build. Mater.* **2023**, *385*, 131508. [CrossRef]
17. Bokaian, A. Natural frequencies of beams under tensile axial loads. *J. Sound Vib.* **1990**, *142*, 481–498. [CrossRef]
18. Spak, K.S.; Agnes, G.S.; Inman, D.J. Modeling vibration response and damping of cables and cabled structures. *J. Sound Vib.* **2015**, *336*, 240–256. [CrossRef]
19. Geuzaine, M.; Foti, F.; Denoël, V. Minimal requirements for the vibration-based identification of the axial force, the bending stiffness and the flexural boundary conditions in cables. *J. Sound Vib.* **2021**, *511*, 116326. [CrossRef]
20. Foti, F.; Geuzaine, M.; Denoël, V. On the identification of the axial force and bending stiffness of stay cables anchored to flexible supports. *Appl. Math. Model.* **2021**, *92*, 798–828. [CrossRef]
21. Park, J. Transfer function methods to measure dynamic mechanical properties of complex structures. *J. Sound Vib.* **2005**, *288*, 57–79. [CrossRef]
22. Ma, Y.; Shi, B.; Ali, L.; Bai, Y.; Fang, P. Mechanical analysis of a type of wire rope subjected to tension. *Ships Offshore Struct.* **2024**, *19*, 541–547. [CrossRef]
23. Rice, W.R. Analyzing tables of statistical tests. *Evolution* **1989**, *43*, 223–225. [CrossRef] [PubMed]